analytical chemistry

Article

pubs.acs.org/ac

Wire, Mesh, and Fiber Electrodes for Paper-Based Electroanalytical Devices

Stephen E. Fosdick, Morgan J. Anderson, Christophe Renault, Paul R. DeGregory, James A. Loussaert, and Richard M. Crooks*

Department of Chemistry and the Center for Nano- and Molecular Science and Technology, The University of Texas at Austin, 105 E. 24th St., Stop A5300, Austin, Texas 78712-1224, United States

Supporting Information

ABSTRACT: Here, we report the use of microwire and mesh working electrodes in paper analytical devices fabricated by origami paper folding (*o*PADs). The important new result is that Au wires and carbon fibers having diameters ranging from micrometers to tens of micrometers can be incorporated into *o*PADs and that their electrochemical characteristics are consistent with the results of finite element simulations. These electrodes are fully compatible with both hollow channels and paper channels filled with cellulose fibers, and they are easier to incorporate than typical screen-printed carbon electrodes. The results also demonstrate that the Au electrodes can be cleaned prior to device fabrication using aggressive treatments and that they can be easily surface modified using standard thiol-based chemistry.

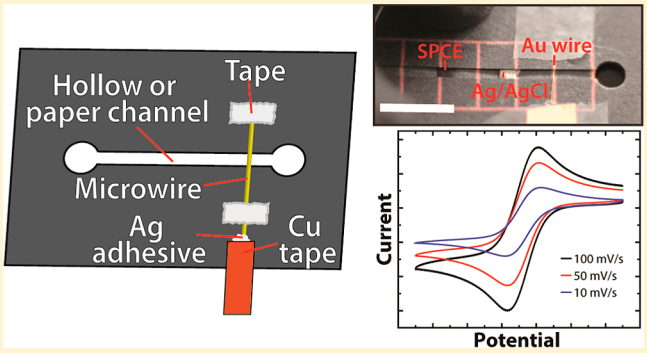

Here, we report paper-based microelectrochemical devices that incorporate conductive wires as electrodes (Scheme 1). The important new result is that the identity and preparation of the wire can be customized to meet the specific requirements of an electrochemical method or assay. This greatly expands the versatility of paper analytical devices (PADs), because at present nearly all PADs employ screen-printed carbon electrodes, which are only partially conductive,[1,2] usually have high surface areas,[3] and are difficult to surface-modify with receptors.[4,5] Additionally, fabrication of PADs incorporating microwire electrodes is significantly easier than current methods for preparing screen-printed electrodes and allows the electrode to be placed at any location within the device. In the present report, we show that Au wires and C fibers can be used as electrodes in PADs based on the principle of origami (*o*PADs). Furthermore, these wire electrodes can be suspended within open channels of paper fluidic devices or between two cellulosic paper channels. Additionally, electrode pretreatments, such as piranha cleaning and modification with self-assembled monolayers (SAMs), can be achieved external to the PAD prior to incorporating them into the device. Finally, this approach makes it possible to change the location of the microwire electrodes and to integrate wire electrodes with screen-printed electrodes when appropriate.

The Whitesides group reported the first examples of two- and three-dimensional fluidic devices built on cellulosic paper platforms.[1,2] Since that time, the intrinsic advantages of paper-based devices, including easy fabrication, low cost, and simple disposal, have led to a renewed interest in paper-based point-of-care (POC) sensing devices.[6−8] Detection in PADs is typically by naked-eye observation of color change,[9−11] fluorescence,[12−14] or electrochemical methods.[4,15−17] Of these, electrochemistry provides a good combination of simplicity, low power requirements, low LODs, and ease of quantitation.[18,19] Indeed, since the first report of electrochemical detection on a PAD by Henry and co-workers, the popularity of this method has rapidly increased.[15,16,20−23] Although nearly all electrodes that have been reported for use in PADs are on the millimeter length scale, there are numerous potential advantages to using smaller dimension electrodes. These include lower capacitances, higher rates of mass transfer, and lower overall currents, leading to reduced ohmic drop (particularly important in PADs) and allowing the use of two-electrode cells.[24,25] Some of these advantages have already been demonstrated by Henry and co-workers, who showed that a microelectrode could be produced in a PAD by creating a hole in a plastic transparency film and filling the resulting hole with C paste.[26]

An unmet need in the field of paper fluidics is the development of better electrode fabrication methods. As mentioned previously, screen-printed carbon electrodes are the current standard for PADs. Such electrodes are produced by pushing a viscous ink containing graphitic carbon suspended in a polymer matrix through a patterned mesh screen or inscribing

Received: January 29, 2014
Accepted: February 27, 2014
Published: March 13, 2014

   dx.doi.org/10.1021/ac5004294 | *Anal. Chem.* 2014, 86, 3659−3666

Scheme 1

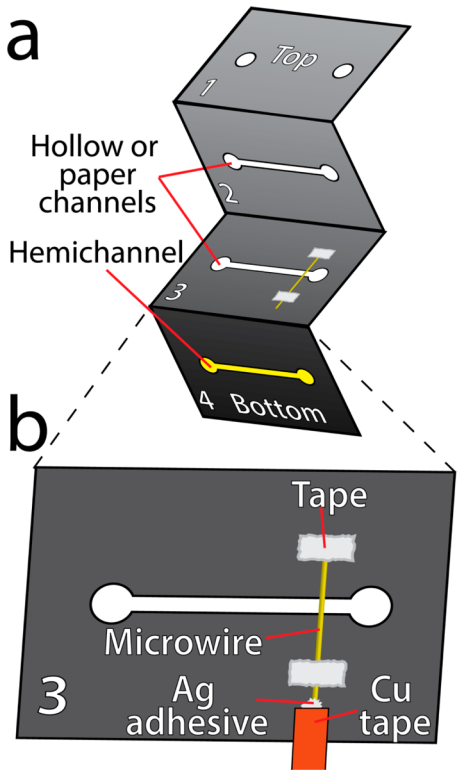

the ink within a stencil to yield a well-defined shape. The primary problems with this approach are the poor electrical properties of the resulting electrodes and their irreproducible surface chemical properties. As an alternative, we propose the use of prefabricated microwire electrodes. Microwires have been used in a variety of electroanalytical systems. For example, Osteryoung and co-workers used C fibers for investigating the electrochemical behavior of *n*-acetylpenicillamine.[27] Henry and co-workers demonstrated postseparation amperometric detection in capillary electrophoresis using a microwire.[28] Additionally, microwires have found use in anodic stripping voltammetry of trace metals.[29,30] The advantages of this type of approach are many but can be summarized on the basis of flexibility in the choice of electrode material, maintaining the ease of device fabrication and rapid prototyping and, perhaps most importantly, the ability to modify electrodes prior to device assembly. Within the context of paper fluidics, this latter advantage is quite similar in concept to our previously reported practice of placing receptors on microbeads,[31] rather than directly modifying cellulose fibers[32,33] or relying on physisorption.[34,35]

EXPERIMENTAL SECTION

Chemicals and Materials. The following chemicals were used as received unless otherwise noted in the text: ferrocenemethanol (FcMeOH) (97%, Sigma-Aldrich), hexaammineruthenium(III) chloride ($Ru(NH_3)_6Cl_3$) (98%, Acros), potassium ferricyanide ($K_3Fe(CN)_6$) (99.99% metals basis, Sigma-Aldrich), potassium nitrate (KNO_3) (99%, EM Sciences), 11-(ferrocenyl)undecanethiol (95%, Sigma-Aldrich), mercaptohexane (Acros), 11-mercaptoundecanoic acid (MUA) (95%, Sigma-Aldrich), ethanol (100%, Capitol Scientific, Austin, TX), hydrogen peroxide (H_2O_2) (30% v/v in H_2O, Fisher Scientific), HPLC grade water (Fisher Scientific), and sulfuric acid (H_2SO_4) (95% H_2SO_4, Fisher Scientific). Whatman grade 1 chromatography paper (20 × 20 cm sheets) was purchased from Fisher Scientific. Au wire (nominal diameter = 0.05 mm, measured diameter = 51.3 ± 0.2 μm, 99.99% Au) was purchased from Alfa-Aesar. Carbon fibers (nominal diameter = 10 μm, measured diameter = 10.0 ± 0.2 μm) were from Goodfellow (Coraopolis, PA). Gold gauze, 100 mesh woven from 0.064 mm diameter wire (99.99%, metals basis), was purchased from Alfa-Aesar. See Figure S1 in the Supporting Information for scanning electron micrographs of the Au wire and C fiber. The carbon (CI-2042) and Ag(83%)/AgCl(17%) (CI-4002) inks were purchased from Engineered Conductive Materials (Delaware, OH). All aqueous solutions were prepared using deionized water (Milli-Q, 18.2 MΩ·cm).

Device Fabrication. The paper channel *o*PADs (PC-*o*PADs) and hollow channel *o*PADs (HC-*o*PADs) were fabricated using a previously reported wax-printing method.[36] The patterns were printed onto Whatman grade 1 chromatographic paper using a Xerox 8570DN inkjet wax printer. After printing, the paper was placed into an oven at 135 °C for 45 s to melt the wax and allow it to spread into the paper matrix. The paper was then cooled to room temperature. HC-*o*PADs were prepared by laser cutting (Epilog Zing 16, Epilog Laser, Golden, CO). The channel dimensions for both PC-*o*PADs and HC-*o*PADs were 1.3 mm wide and 30 mm long. The channels consist of two paper layers, making the final channel height ~0.35 mm.

Au wire electrodes were cleaned by immersion in piranha solution (1:3 H_2O_2/H_2SO_4) for 1 min and then water immediately prior to use. *Caution: piranha solution is a strong oxidant and reacts violently with organic materials. It should be handled with extreme care; all work should be performed under a fume hood and with protective gear.* The C fiber was used as received. Ag conductive adhesive (Electron Microscopy Sciences) and Cu tape (3M) were used to make electrical contact to the microwires. The wires were placed ~5 mm from the outlet reservoir of the *o*PAD to reduce ohmic drop during electrochemical experiments (in most cases, the reference and counter electrodes were placed in the outlet reservoir). Photographs showing the device and the wire placement are provided in the Supporting Information.

In some cases, *o*PAD configurations were tested in which the working, counter, and reference electrodes were all present within the HC-*o*PAD. In this case, the counter and reference electrodes were stencil-printed onto the bottom of Layer 1 (Scheme 1) by pushing carbon ink through a mask, which was a laser-cut plastic transparency. Before stencil-printing, the ink was heated and uncovered, for 30 min in an oven set to 65 °C. After letting the ink cool to room temperature, a scraper was used to push the ink through the mask onto the HC-*o*PAD. The HC-*o*PAD was then cured at 65 °C for 90 min. After curing the carbon ink, Ag/AgCl paste was painted onto one of the stencil-printed electrodes and it was cured at 65 °C for 30 min. The front edge of the Ag/AgCl quasi-reference electrode (QRE) was configured to be 5 mm from the microwire, and the back edge of the counter electrode was situated 15 mm from the microwire. Both the counter and quasi-reference electrodes spanned the width of the hollow channel, and their lengths were 3 mm. A portion of the screen-printed carbon extended beyond the channel to facilitate electrical contact.

All devices were folded into the final configuration prior to being sandwiched between two rigid, 5-mm thick acrylic holders, which were clamped with binder clips. In the case of

dx.doi.org/10.1021/ac5004294 | *Anal. Chem.* 2014, 86, 3659−3666

HC devices, when solution was added to the cell, the flow was stabilized by adding small additions of solution to the inlet or outlet during the first ~5 min. After that, the cell was allowed to equilibrate for another 10−20 min to reduce the flow rate within the channel. For all experiments described here, this procedure was followed and no flow was intentionally induced.

Preparation of SAM-Coated Au Microwires. The Au wire electrodes were cleaned by immersion in piranha solution for 1 min, followed by rinsing in HPLC-grade water. The wires were then immersed in an ethanolic solution of 2.5 mM MUA for 48 h, to create a SAM having a negatively charged terminus, or in a solution of 1.0 mM 11-(ferrocenyl)undecanethiol and 1.0 mM mercaptohexane for 1 h, to prepare electroactive SAMs. The wires were removed from the thiol solutions and dipped into clean ethanol to remove any unbound thiols. The *o*PADs where then assembled as previously described.

Electrochemical Measurements. Electrochemical measurements were carried out at 23 ± 2 °C using a potentiostat (Model 650C or 700E, CH Instruments, Austin, TX). Unless otherwise indicated, the reference electrode was a mercury/mercurous sulfate electrode (MSE) (Hg/Hg_2SO_4 sat'd K_2SO_4, E = 0.64 V vs NHE) and the counter electrode was a Pt wire or mesh. Most electrochemical measurements were carried out using a solution consisting of 1.0 mM FcMeOH and 0.10 M KNO_3. For electrochemical experiments using a MUA SAM-coated working electrode, solutions containing either 1.0 mM $Ru(NH_3)_6^{3+}$ and 0.10 M KNO_3 or 1.0 mM $Fe(CN)_6^{3-}$ and 0.10 M KNO_3 were used. In some cases, data were smoothed using a 5-point moving average to reduce noise.

Finite Element Simulations. Finite element simulations were performed using a Dell Precision T7500 workstation equipped with Dual Six Core Intel Xeon Processors (2.40 GHz) and 24 GB of RAM. Simulations were performed using the COMSOL Multiphysics v4.3b commercial package. All simulations were performed using a 2D geometry. The simulation geometry was made of a rectangle 360 μm (h) × 1 mm (w) with a circle representing the wire electrode placed in the center of the channel and subtracted from the geometry (see Figures S2 and S3 in the Supporting Information). The geometry was then cut in half along the vertical axis of symmetry to reduce computation time. An extremely fine mesh was placed over the electrode surface such that the maximum element size was 50 nm. A boundary layer mesh, consisting of 8 layers, was also placed over the electrode surface. The total number of mesh elements was 103,760 for the C fiber and 291,704 for Au wire. The largest mesh element in both cases was 10 μm.

Electrochemistry was modeled using the "Transport of Diluted Species" COMSOL module. Both FcMeOH and the oxidized form, ferroceniummethanol, $FcMeOH^+$, were considered for each calculation. The electrochemical reaction of the redox probe is described by eq 1.

$$FcMeOH^+ + e^- \leftrightarrow FcMeOH \tag{1}$$

The model assumed Butler−Volmer kinetics at the electrode surface.[24] This kinetic model dictates the rates of the forward (reduction) and back (oxidation) reactions based on eqs 2 and 3.

$$k_F = k^\circ \exp\left[\frac{F\alpha(E - E^\circ)}{RT}\right] \tag{2}$$

$$k_B = k^\circ \exp\left[\frac{F(1 - \alpha)(E - E^\circ)}{RT}\right] \tag{3}$$

where F is the Faraday constant (96,485 C mol^{-1}), R is the gas constant (8.314 J mol^{-1} K^{-1}), T is the temperature (298.15 K), E° is the standard reduction potential for the redox couple (−0.20 V vs MSE based on experimental observation), E is the potential of the electrode, k° is the standard kinetic rate constant (0.2 cm s^{-1}),[37] α is the transfer coefficient (0.5),[37] and k_F and k_B are the forward and backward rates of the reaction at the electrode surface, respectively. On the basis of these equations, it was possible to set the boundaries of the electrode surface as "Flux Boundaries" such that the flux into the solution domain across the electrode surface (N) is given by eqs 4 and 5.

$$N_{FcMeOH^+} = k_B c_{FcMeOH} - k_F c_{FcMeOH^+} \tag{4}$$

$$N_{FcMeOH} = -N_{FcMeOH^+} = k_F c_{FcMeOH^+} - k_B c_{FcMeOH} \tag{5}$$

The floor and the ceiling of the simulation geometry were taken to be no flux boundaries. Boundaries adjacent to the electrode were taken to be symmetry boundaries. The remaining boundary was taken to be a concentration boundary, such that c_{FcMeOH} = 1 mM and $c_{FcMeOH+}$ = 0 mM.

All simulations were performed under no-flow conditions, so the effects of convection and electromigration terms were neglected. Consequently, mass transfer is defined by eq 6.

$$N = -D\nabla c \tag{6}$$

Transient simulated cyclic voltammograms were obtained by varying the value of E as a function of time, while simulated chronoamperometric traces (i−t) were obtained by fixing E for the entire time window. In each case, the current at the electrode surface was calculated using eq 7.

$$i = 2FWN^{norm}_{FcMeOH^+} \tag{7}$$

where W is the channel width (1.3 mm) and $N^{norm}_{FcMeOH^+}$ is the normal flux of $FcMeOH^+$ integrated across the electrode surface. A factor of 2 is included to account for the symmetry of the system.

RESULTS AND DISCUSSION

Device Platform and Considerations for Electroanalysis. The general design used in these experiments is illustrated in Scheme 1. The device is fabricated using the folding principles of origami to create a multilayered structure we call an *o*PAD.[21,38] Two types of channels were used: (1) typical paper channels (PCs) filled with cellulose fibers and defined using wax printing[12,39] and (2) HCs fabricated using a laser cutter to remove a section of cellulose fibers.[36] We have previously shown that HCs have a number of desirable characteristics, including simple fabrication, increased fluid flow, reduced surface area available for nonspecific adsorption, and reproducible electrochemical characteristics.[40] As shown in Scheme 1, Layer 1 contains an inlet and outlet. Layers 2 and 3 contain two stacked channels, which may be either hollow or filled with cellulose fibers. The bottom layer contains a feature of similar dimensions to the channels in Layers 2 and 3, but which is partially waxed. We call this type of structure a hemichannel.[36] It consists of a top layer (~70 μm) of cellulose fibers and a bottom layer (~110 μm) of wax-filled cellulose. Both layers are present within a single ~180 μm-thick section of the constituent paper. The hydrophilic layer of the hemichannels enables capillary flow in HCs.[36,41]

dx.doi.org/10.1021/ac5004294 | Anal. Chem. 2014, 86, 3659−3666

The *o*PAD platform depicted in Scheme 1 allows microwires to be placed anywhere within the channels of either a HC or PC device. However, in most cases discussed herein (and unless otherwise stated), the microwires were placed between Layers 2 and 3, as shown in Scheme 1a, resulting in a wire suspended at the vertical center of the channel. Wires can also be placed on the top of the channel (bottom of Layer 1) in a HC-*o*PAD. Additionally, the wire can be placed between two paper channels (Layers 2 and 3) in a PC-*o*PAD. Examples of these types of device configurations can be found in the Supporting Information (Figures S4 and S5).

For electrochemical detection schemes where the analyte is a freely diffusing species, it is advantageous to reach steady-state mass transport conditions, such as radial diffusion to an ultramicroelectrode.[24] This is because the steady state simplifies the relationship between current and concentration of a redox target.[24] Micron-scale wires can achieve a quasi-steady state current response even in nonflowing solutions. On the other hand, many detection schemes rely on an electrode-immobilized receptor probe, such as single-stranded DNA or an antibody. In this case, it may be desirable to use electrodes having higher surface areas than a micrometer-scale wire can provide. Later, we will show that the flexibility of the approach described here provides for this need too.

Electrochemistry at Microwire Electrodes. Figure 1 shows a series of experimentally obtained cyclic voltammograms (CVs) (black lines) overlaid onto simulated CVs (red circles). These data were collected using a quiescent electrolyte solution consisting of 1.0 mM FcMeOH and 0.10 M KNO_3 and scan rates (ν) of 10, 50, and 100 mV/s. For this data set, the working electrode was a 51.3 μm-diameter Au wire stretched across Layer 3 of a HC-*o*PAD (Scheme 1) and placed 5 mm from the outlet reservoir. Because there is a HC above and below the wire, this results in the electrode being configured at the vertical center of the channel.

The CVs in Figure 1 are typical of a reversible redox couple subject to scan-rate-dependent mass transfer conditions at a cylindrical microelectrode.[25,42] That is, at a scan rate of 100 mV/s, the peak-shaped voltammogram is qualitatively characteristic of linear diffusion, but as the scan rate is lowered, the peak-shaped feature flattens and starts to become more characteristic of radial diffusion.

To better understand the voltammetric response of the device shown in Figure 1, we carried out finite element simulations (FES, red circles). While analytical solutions of the current response at microwire electrodes have been presented,[42,43] the unique geometry of the *o*PAD, such as the impact of the top and bottom of the channel on resulting concentration profiles, necessitates consideration of the location of the electrode in the device. As seen in Figure 1, the shapes of the experimental and simulated results have the same general characteristics, and the current magnitudes are in semiquantitative agreement with one-another. For example, differences in the anodic peak currents ($i_{p,a}$) are typically within 7−16% depending on the scan rate. This variation is on the same order as the device-to-device variation in $i_{p,a}$ observed for nominally identical *o*PADs and experimental conditions (~10%, Figure S6 in the Supporting Information). One significant difference between the experimental and simulated CVs relates to the uncompensated resistance (R_u) present in the *o*PAD. The experimental data in Figure 1 were not corrected for R_u, which has a measured value of 6.3 ± 0.2 kΩ. R_u results in a larger peak splitting (ΔE_p = 90−100 mV, depending upon scan rate) than is observed in the simulations (ΔE_p = 78−90 mV).

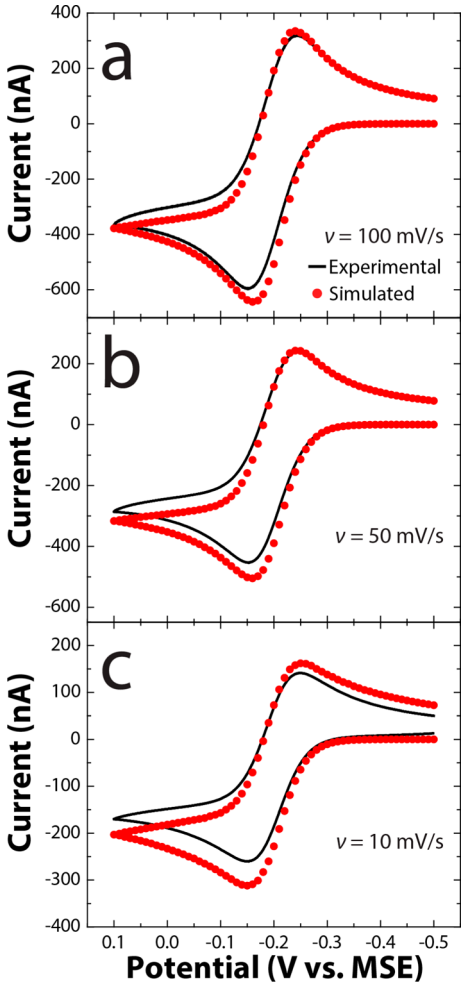

Figure 1. CVs of a 1.0 mM FcMeOH solution obtained using a 51.3 μm diameter Au wire working electrode in a HC-*o*PAD, like that depicted in Scheme 1, at scan rates between 10 and 100 mV/s. The black lines show the experimental results, and the filled red circles are the results of finite element simulations. The Au wire was situated 5 mm from the outlet of the channel and was placed between Layers 2 and 3 of the device. This results in a configuration where the microwire electrode is suspended at the half height (vertical center) of the channel. The supporting electrolyte was 0.10 M KNO_3.

Figure 2 shows a series of CVs obtained at different scan rates using a 10.0 μm C fiber working electrode. In all other respects, the conditions are the same as those used to obtain the data in Figure 1. In this case, however, the simulated and experimental results are in better agreement (<6% difference) than for the larger Au wire electrode. This might be a consequence of the C fiber being more rigid than the Au wire, which can deform or bend during assembly of the *o*PAD. Additionally, because of the smaller radial dimension, the voltammetry at the C fiber electrodes exhibits less contribution from linear diffusion than does the larger Au wire. Accordingly, one advantage of the C fiber over the Au wire is that the smaller radial dimension leads to shorter time requirements for entering the quasi-steady state mass transfer regime. Examples of chronoamperometric experiments collected in HC-PADs with Au wire and C fiber can be found in Figure S7 in the Supporting Information.

dx.doi.org/10.1021/ac5004294 | *Anal. Chem.* 2014, 86, 3659−3666

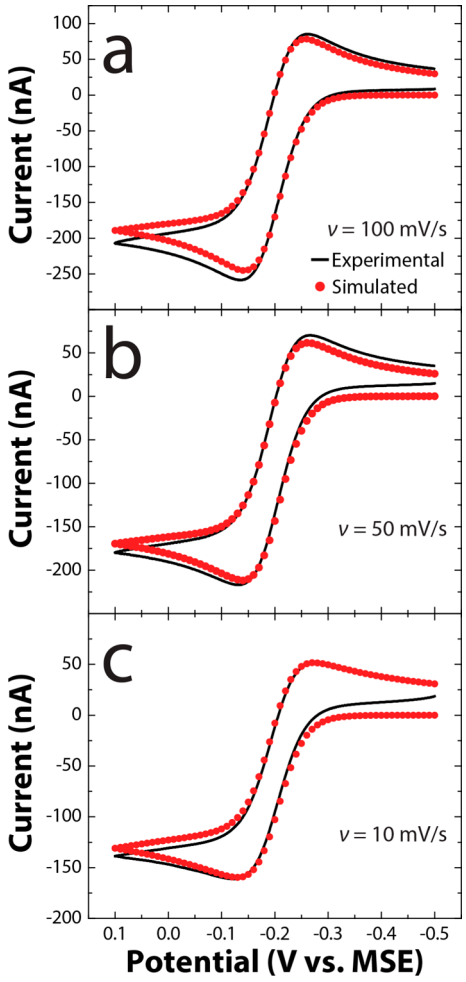

Figure 2. CVs of a 1.0 mM FcMeOH solution obtained using a 10.0 μm diameter C fiber working electrode in a HC-*o*PAD, like that depicted in Scheme 1, at scan rates between 10 and 100 mV/s. The black lines show the experimental results, and the red circles show the results of finite element simulations. The C fiber was situated 5 mm from the outlet of the channel and was placed between Layers 2 and 3 of the device. This results in a configuration where the microwire electrode is suspended at the half height (vertical center) of the channel. The supporting electrolyte was 0.10 M KNO_3.

Modification of Au Wire with SAMs. One important advantage of using wires as electrodes in PADs, rather than screen-printed electrodes, is that the former can be surface modified, for example, with a bioreceptor, just prior to device assembly. This means that cleaning procedures that would destroy the paper or the hydrophobic wax support (e.g., piranha cleaning, ethanol washes) can be carried out. An additional advantage of wires over screen-printed electrodes is that a long length of wire can be modified simultaneously and subsequently cut into pieces and inserted into the *o*PAD. Finally, because paper swells in water and because water penetrates wax on a time scale of tens of minutes,[40] long electrode modification times are impractical for screen-printed electrodes on paper.

Figure 3 provides an example of some of the advantages alluded to in the previous paragraph. Figure 3a shows 20 consecutive CVs obtained at a scan rate of 100 mV/s and using a Au wire working electrode that was piranha-cleaned and then exposed to an ethanolic solution containing 1.0 mM 11-(ferrocenyl)undecanethiol and 1.0 mM mercaptohexane for 1 h prior to being configured in the *o*PAD with a 0.10 M KNO_3 electrolyte solution. Clearly, the scan-to-scan variability is small and consistent with published results obtained in more traditional electrochemical cells.[44−47] Figure 3b shows the voltammetric response of the same electrode but at scan rates ranging from 50 to 250 mV/s. Because the film is immobilized on the electrode, the magnitude of the peak currents should vary linearly with scan rate.[24] The inset of Figure 3b shows that this behavior is observed for the electroactive SAM for both the anodic and cathodic peaks.

The wire electrodes can also be modified with SAMs that selectively block particular redox couples. For instance, when a thiolated SAM having a distal carboxylic acid group is immobilized on a Au electrode and the pH of the electrolyte solution is above the pK_a of the acid, then a negatively charged interface develops. This negative charge can then interact electrostatically with diffusing redox species and either promote or suppress their ability to undergo electron transfer.

Figure 3c shows CVs of the reduction of $Ru(NH_3)_6^{3+}$ at a naked Au wire (black) and one modified with an acid-terminated MUA SAM (red). The naked Au wire exhibits current due to simultaneous reduction of both oxygen (at potentials more negative than −0.5 V vs MSE) and $Ru(NH_3)_6^{3+}$. The MUA SAM results in three major changes to the voltammetry of the $Ru(NH_3)_6^{3+}$ at the Au wire electrode: (1) the background current due to oxygen reduction is suppressed, (2) $Ru(NH_3)_6^{3+}$ reduction is shifted to more negative potentials, and (3) the reoxidation of electroreduced $Ru(NH_3)_6^{2+}$ is suppressed. The decrease in current contributions from oxygen reduction and the shift to slightly more negative potentials for $Ru(NH_3)_6^{3+}$ reduction are a consequence of the SAM blocking the Au surface, the increased resistance of electron tunneling through the SAM, and the change in the interfacial potential induced by the charged terminus of the SAM.[48,49] The apparent quasi-reversible or irreversible voltammetric behavior has been previously observed with oppositely charged SAM/redox probe systems.[48,50−53] The effect may be due in part to the effective interfacial potential difference caused by the charged SAM as well as the effect of the SAM on the distribution of ions at the interface.

Figure 3d shows CVs obtained at a naked Au wire electrode (black) and a Au wire modified with a MUA SAM (red) in a solution containing 1.0 mM $Fe(CN)_6^{3-}$ and 0.10 M KNO_3. In contrast to the response of the $Ru(NH_3)_6^{3+}$ solution, where the redox probe is a positively charged species, $Fe(CN)_6^{3-}$ is negatively charged and the electrostatic interaction between the MUA SAM and $Fe(CN)_6^{3-}$ prevents significant electron transfer.[48,54,55] Therefore, the voltammetric response of the electrode exhibits very little faradaic current (<0.6% of the peak current of the naked Au wire). The electrochemical results obtained using these modified Au electrodes demonstrate the likely utility of wire electrodes in future PAD-based sensors.

Fully Integrated Device. Because electrochemical PADs are intended primarily for POC applications, it is important that they be functional in a fully integrated format. The results discussed in this section demonstrate that all three electrodes required for voltammetry can be placed within a hollow channel and that the electrochemical results are nearly identical to those obtained when the reference and counter electrodes are situated outside of the device.

Figure 4a shows a picture of a HC-*o*PAD incorporating 3 electrodes: a Au microwire working electrode, a SPCE coated

dx.doi.org/10.1021/ac5004294 | *Anal. Chem.* 2014, 86, 3659−3666

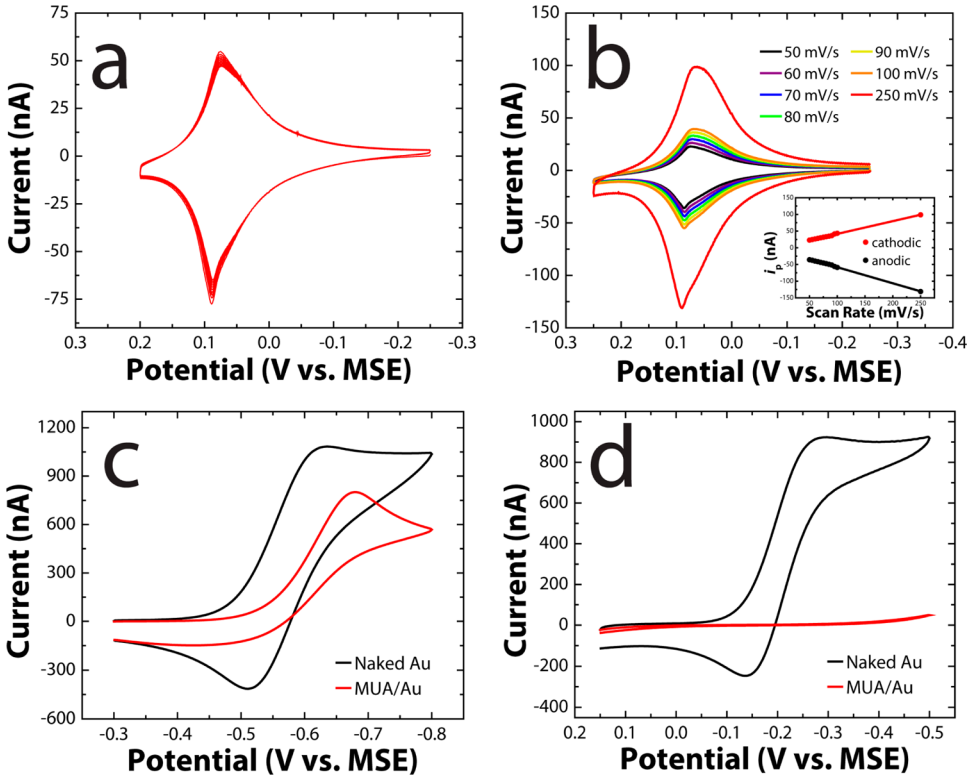

Figure 3. (a) Twenty consecutive CVs obtained using a 51.3 μm Au wire electrode comodified with 11-(ferrocenyl)undecanethiol and mercaptohexane at a scan rate of 100 mV/s. (b) CVs of the SAM in (a) at scan rates ranging between 50 and 250 mV/s. The inset is a plot of $i_{p,a}$ and $i_{p,c}$ vs scan rate. (c) CVs obtained using a naked 51.3 μm Au wire (black) and a Au wire modified with a MUA SAM (red) in a solution containing 1.0 mM $Ru(NH_3)_6^{3+}$ and 0.10 M KNO_3 at a scan rate of 100 mV/s. (d) CVs obtained using a naked Au wire (black) and a Au wire modified with a MUA SAM (red) in a solution containing 1.0 mM $Fe(CN)_6^{3-}$ and 0.10 M KNO_3 at a scan rate of 100 mV/s.

with Ag/AgCl paste serving as a QRE, and a SPCE counter electrode. This device was tested in 1.0 mM FcMeOH containing 0.10 M KNO_3. The resulting voltammetry, shown in Figure 4b, is very similar to the results obtained when the reference and counter electrode are placed in the outlet reservoir of the device. The levels of R_u are also comparable: 6–10 kΩ.

Figure 4c compares amperometric i–t curves collected using 4 independently fabricated, fully integrated devices with simulated results. The average quasi-steady state currents (i_{qss}) for these 4 devices at 30 and 60 s were −178 ± 18 and −154 ± 13 nA, respectively. The corresponding simulated values of i_{qss} at 30 and 60 s were −201 and −154 nA, respectively. The key point is that the function of the *o*PAD is independent of the location of the three electrodes regardless of the electrochemical method (voltammetry or amperometry) employed.

Additional Electrode Configurations. The platform design shown in Scheme 1 provides a flexible means for positioning working electrodes in configurations other than those described thus far. For example, Figure S4 in the Supporting Information provides a photograph of an *o*PAD in which the Au wire working electrode is placed at the top of a hollow channel (bottom side of Layer 1) instead of at the half height (between Layers 2 and 3). The resulting voltammetry is reproducible and consistent with expectations. Figure S5 in the Supporting Information shows that both Au wire and C fiber electrodes are also fully functional when incorporated into cellulose-filled paper channels. Finally, Figure S8 in the Supporting Information demonstrates that a Au mesh electrode can also be integrated into HC-*o*PAD devices. This type of electrode provides additional surface area, compared to a single wire, and hence could be useful for immobilization of bioprobes, such as DNA or antibodies.

SUMMARY AND CONCLUSIONS

We have shown that Au microwires and meshes, as well as C fibers, can be used as working electrodes within paper-based electroanalytical devices. The voltammetric responses of these electrodes are consistent with finite element simulations, and hence, their behavior is easily predictable, even when reference and counter electrodes are integrated within the paper platform. Mesh electrodes provide higher surface areas than wires and could be useful for applications requiring higher surface areas for immobilization of bioprobes. Although this report has focused on just Au and C electrodes, there is no obvious barrier to using other common electrode materials such as Pt or even Hg-thin film electrodes.

Heretofore, most working electrodes in PADs have been based on carbon inks, but depending on the application, wires, fibers, and meshes may provide some distinct advantages. For example, they can be more easily cleaned and modified and may well be easier to integrate, using pick and place methods, than screen- or stencil-printed electrodes. In the future, we intend to explore how these types of electrodes can be used to address specific electroanalytical needs for POC sensors. The results of these studies will be reported in due course.

dx.doi.org/10.1021/ac5004294 | *Anal. Chem.* 2014, 86, 3659–3666

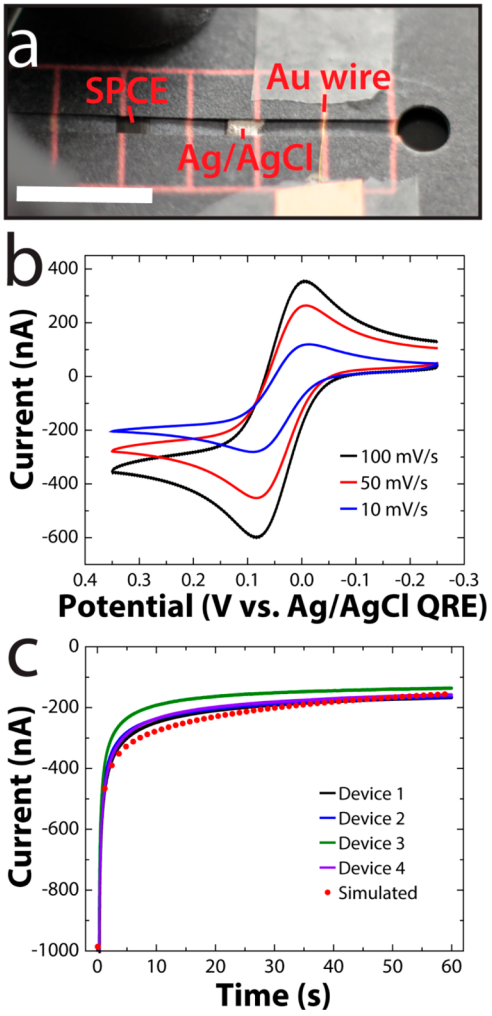

Figure 4. (a) Photograph of a fully integrated *o*PAD wherein the working electrode is a 51.3 μm Au wire, the reference electrode is a SPCE coated with Ag/AgCl paste, and the counter electrode is a SPCE. The pink lines are alignment marks used to accurately fold the device and to achieve reproducible electrode placement. The white scale bar indicates 1.00 cm. (b) CVs of 1.0 mM FcMeOH obtained using the *o*PAD shown in (a) at scan rates between 10 and 100 mV/s. The electrolyte was 0.10 M KNO_3. (c) Chronoamperometry of 1.0 mM FcMeOH using four independently fabricated *o*PADs like that shown in (a). The potential of the Au wire working electrode was stepped from −0.25 to 0.35 V vs Ag/AgCl QRE for 60 s. The corresponding finite element simulation is also shown (filled red circles). In all cases, the electrolyte was 0.10 M KNO_3.

■ ASSOCIATED CONTENT

Ⓢ Supporting Information

Scanning electron micrographs of Au wire and C fiber electrodes, finite element simulations, demonstration of the voltammetric reproducibility of Au wire and C fiber electrodes in *o*PADs, and detailed information about alternative electrodes and electrode configurations. This material is available free of charge via the Internet at http://pubs.acs.org.

■ AUTHOR INFORMATION

Corresponding Author

*E-mail: crooks@cm.utexas.edu.

Notes

The authors declare no competing financial interest.

■ ACKNOWLEDGMENTS

This project is sponsored by the Department of the Defense, Defense Threat Reduction Agency (contract number HDTRA-1-13-1-0031). The content of the information does not necessarily reflect the position or the policy of the federal government, and no official endorsement should be inferred. We thank Prof. Allen J. Bard for the use of the C fiber electrodes. R.M.C. thanks the Robert A. Welch Foundation (Grant F-0032) for sustained research support.

■ REFERENCES

(1) Wang, J.; Tian, B.; Nascimento, V. B.; Angnes, L. *Electrochim. Acta* **1998**, *43*, 3459−3465.
(2) Fanjul-Bolado, P.; Hernández-Santos, D.; Lamas-Ardisana, P. J.; Martín-Pernía, A.; Costa-García, A. *Electrochim. Acta* **2008**, *53*, 3635−3642.
(3) Töbjork, D.; Österbacka, R. *Adv. Mater.* **2011**, *23*, 1935−1961.
(4) Ge, S.; Ge, L.; Yan, M.; Song, X.; Yu, J.; Huang, J. *Chem. Commun.* **2012**, *48*, 9397−9399.
(5) Wu, Y.; Xue, P.; Hui, K. M.; Kang, Y. *Biosens. Bioelectron.* **2014**, *52*, 180−187.
(6) Li, X.; Ballerini, D. R.; Shen, W. *Biomicrofluidics* **2012**, *6*, 11301.
(7) Parolo, C.; Merkoci, A. *Chem. Soc. Rev.* **2013**, *42*, 450−457.
(8) Yetisen, A. K.; Akram, M. S.; Lowe, C. R. *Lab Chip* **2013**, *13*, 2210−2251.
(9) Dungchai, W.; Chailapakul, O.; Henry, C. S. *Anal. Chim. Acta* **2010**, *674*, 227−33.
(10) Vella, S. J.; Beattie, P.; Cademartiri, R.; Laromaine, A.; Martinez, A. W.; Phillips, S. T.; Mirica, K. A.; Whitesides, G. M. *Anal. Chem.* **2012**, *84*, 2883−2891.
(11) Mentele, M. M.; Cunningham, J.; Koehler, K.; Volckens, J.; Henry, C. S. *Anal. Chem.* **2012**, *84*, 4474−4480.
(12) Carrilho, E.; Phillips, S. T.; Vella, S. J.; Martinez, A. W.; Whitesides, G. M. *Anal. Chem.* **2009**, *81*, 5990−5998.
(13) Allen, P. B.; Arshad, S. A.; Li, B.; Chen, X.; Ellington, A. D. *Lab Chip* **2012**, *12*, 2951−2958.
(14) Scida, K.; Li, B.; Ellington, A. D.; Crooks, R. M. *Anal. Chem.* **2013**, *85*, 9713−9720.
(15) Dungchai, W.; Chailapakul, O.; Henry, C. S. *Anal. Chem.* **2009**, *81*, 5821−5826.
(16) Carvalhal, R. F.; Simão Kfouri, M.; de Oliveira Piazetta, M. H.; Gobbi, A. L.; Kubota, L. T. *Anal. Chem.* **2010**, *82*, 1162−1165.
(17) Noiphung, J.; Songjaroen, T.; Dungchai, W.; Henry, C. S.; Chailapakul, O.; Laiwattanapaisal, W. *Anal. Chim. Acta* **2013**, *788*, 39−45.
(18) Nie, Z.; Deiss, F.; Liu, X.; Akbulut, O.; Whitesides, G. M. *Lab Chip* **2010**, *10*, 3163−3169.
(19) Maxwell, J. E.; Mazzeo, A. D.; Whitesides, G. M. *MRS Bull.* **2013**, *38*, 309−314.
(20) Nie, Z.; Nijhuis, C. A.; Gong, J.; Chen, X.; Kumachev, A.; Martinez, A. W.; Narovlyansky, M.; Whitesides, G. M. *Lab Chip* **2010**, *10*, 477−483.
(21) Liu, H.; Xiang, Y.; Lu, Y.; Crooks, R. M. *Angew. Chem., Int. Ed.* **2012**, *51*, 6925−6928.
(22) Thom, N. K.; Yeung, K.; Pillion, M. B.; Phillips, S. T. *Lab Chip* **2012**, *12*, 1768−1770.
(23) Wang, P.; Ge, L.; Yan, M.; Song, X.; Ge, S.; Yu, J. *Biosens. Bioelectron.* **2012**, *32*, 238−243.
(24) Bard, A. J.; Faulkner, L. R. *Electrochemical Methods: Fundamentals and Applications*, 2nd ed.; John Wiley & Sons: New York, 2001.
(25) Michael, A. C.; Wightman, R. M. Microelectrodes. In *Laboratory Techniques in Electroanalytical Chemistry*, 2nd ed, Revised and Expanded; Kissinger, P., Heineman, W.R., Eds; Marcel Dekker, Inc.: New York, 1996; p 367−402.
(26) Santhiago, M.; Wydallis, J. B.; Kubota, L. T.; Henry, C. S. *Anal. Chem.* **2013**, *85*, 5233−5239.

(27) Nuwer, M. J.; Osteryoung, J. *Anal. Chem.* **1989**, *61*, 1954−1959.
(28) Liu, Y.; Vickers, J. A.; Henry, C. S. *Anal. Chem.* **2004**, *76*, 1513−1517.
(29) Salaün, P.; Gibbon-Walsh, K.; van den Berg, C. M. G. *Anal. Chem.* **2011**, *83*, 3848−3856.
(30) Alves, G. M. S.; Magalhães, J. M. C. S.; Tauler, R.; Soares, H. M. V. M. *Electroanalysis* **2013**, No. 25, 1895−1906.
(31) Liu, H.; Xiang, Y.; Lu, Y.; Crooks, R. M. *Angew. Chem., Int. Ed.* **2012**, *51*, 6925−6928.
(32) Yu, A.; Shang, J.; Cheng, F.; Paik, B. A.; Kaplan, J. M.; Andrade, R. B.; Ratner, D. M. *Langmuir* **2012**, *28*, 11265−11273.
(33) Araújo, A. C.; Song, Y.; Lundeberg, J.; Ståhl, P. L.; Brumer, H. *Anal. Chem.* **2012**, *84*, 3311−3317.
(34) Cheng, C.-M.; Martinez, A. W.; Gong, J.; Mace, C. R.; Phillips, S. T.; Carrilho, E.; Mirica, K. A.; Whitesides, G. M. *Angew. Chem., Int. Ed.* **2010**, *49*, 4771−4774.
(35) Wang, P.; Ge, L.; Ge, S.; Yu, J.; Yan, M.; Huang, J. *Chem. Commun.* **2013**, *49*, 3294−3296.
(36) Renault, C.; Li, X.; Fosdick, S. E.; Crooks, R. M. *Anal. Chem.* **2013**, *85*, 7976−7979.
(37) Cannes, C.; Kanoufi, F.; Bard, A. J. *J. Electroanal. Chem.* **2003**, *547*, 83−91.
(38) Liu, H.; Crooks, R. M. *J. Am. Chem. Soc.* **2011**, *133*, 17564−17566.
(39) Lu, Y.; Shi, W.; Jiang, L.; Qin, J.; Lin, B. *Electrophoresis* **2009**, *30*, 1497−1500.
(40) Renault, C.; Anderson, M. J.; Crooks, R. M. *J. Am. Chem. Soc.* **2014**, DOI: 10.21021/ja4118544.
(41) Glavan, A. C.; Martinez, R. V.; Maxwell, E. J.; Subramaniam, A. B.; Nunes, R. M. D.; Soh, S.; Whitesides, G. M. *Lab Chip* **2013**, *13*, 2922−2930.
(42) Molina, A.; Gonzalez, J.; Henstridge, M. C.; Compton, R. G. *J. Phys. Chem. C* **2011**, *115*, 4054−4062.
(43) Szabo, A.; Cope, D. K.; Tallman, D. E.; Kovach, P. M.; Wightman, R. M. *J. Electroanal. Chem. Interfacial Electrochem.* **1987**, *217*, 417−423.
(44) Chidsey, C. E. D.; Bertozzi, C. R.; Putvinski, T. M.; Mujsce, A. M. *J. Am. Chem. Soc.* **1990**, *112*, 4301−4306.
(45) Collard, D. M.; Fox, M. A. *Langmuir* **1991**, *7*, 1192−1197.
(46) Uosaki, K.; Sato, Y.; Kita, H. *Langmuir* **1991**, *7*, 1510−1514.
(47) Cruanes, M. T.; Drickamer, H. G.; Faulkner, L. R. *Langmuir* **1995**, *11*, 4089−4097.
(48) Takehara, K.; Takemura, H.; Ide, Y. *Electrochim. Acta* **1994**, *39*, 817−822.
(49) Cattabriga, M.; Ferri, V.; Tran, E.; Galloni, P.; Rampi, M. A. *Inorg. Chim. Acta* **2007**, *360*, 1095−1101.
(50) Sun, L.; Johnson, B.; Wade, T.; Crooks, R. M. *J. Phys. Chem.* **1990**, *94*, 8869−8871.
(51) Tokuhisa, H.; Zhao, M.; Baker, L. A.; Phan, V. T.; Dermody, D. L.; Garcia, M. E.; Peez, R. F.; Crooks, R. M.; Mayer, T. M. *J. Am. Chem. Soc.* **1998**, *120*, 4492−4501.
(52) Yang, M.; Zhang, Z. *Electrochim. Acta* **2004**, *49*, 5089−5095.
(53) Campiña, J. M.; Martins, A.; Silva, F. *J. Phys. Chem. C* **2009**, *113*, 2405−2416.
(54) Pardo-Yissar, V.; Katz, E.; Lioubashevski, O.; Willner, I. *Langmuir* **2001**, *17*, 1110−1118.
(55) Bradbury, C. R.; Zhao, J. J.; Fermin, D. J. *J. Phys. Chem. C* **2008**, *112*, 10153−10160.